Applied Catalysis B: Environmental 202 (2017) 134–146

Contents lists available at ScienceDirect

Applied Catalysis B: Environmental

journal homepage: www.elsevier.com/locate/apcatb

In-situ incorporation of binder during sol-gel preparation of Pd-based sulfated zirconia for reduction of nitrogen oxides under lean-burn conditions: Effect on activity and wash-coating characteristics

Sreshtha Sinha Majumdar, Gokhan Celik, Anne-Marie Alexander, Preshit Gawade, Umit S. Ozkan*

The Ohio State University, United States

ARTICLE INFO

Article history:
Received 16 June 2016
Received in revised form 26 August 2016
Accepted 29 August 2016
Available online 30 August 2016

Keywords:
NO_x reduction
Lean-burn
Sulfated zirconia
Alumina binder
Wash-coat
Sol-gel

ABSTRACT

We have developed a dual-catalyst aftertreatment system for reducing nitrogen oxides (NO_x) in the exhaust stream of natural gas-fired lean-burn engines by utilizing the unburned hydrocarbons present in the engine exhaust. The dual-catalyst bed consists of a physical mixture of a reduction catalyst (Pd/SZ) and an oxidation catalyst (Co/CeO_2). In order to make this dual-catalyst system viable for practical use in the real aftertreatment units, it is necessary to develop a catalytically active washcoat for loading it onto cordierite monolith cores. To be able to handle large throughputs of gases typical of aftertreatment units, irreversible loss of activity due to separation of the wash-coat from the monolith walls can be reduced by adding binders to improve the adhesive properties of the wash-coat. However, addition of such binders may affect the catalytic activity of the resulting dual-catalyst bed. In our study, we have incorporated binders such as alumina, boehmite, bentonite or silica to the Pd/SZ catalyst using a novel technique in which the binders were added in situ during the sol-gel synthesis rather than the conventional method of adding binders (ex-situ) in catalyst slurry. Surface area analysis, X-ray diffraction (XRD) and diffuse reflectance Fourier transform spectroscopy (DRIFTS) with pyridine show that in-situ addition of binder affects the textural properties, crystal phase of zirconia and the acidic properties of the resulting Pd/SZ catalyst respectively. Electron Paramagnetic Resonance (EPR) indicated the presence of Pd^{+}, Pd^{3+} and Zr^{3+} species in the binder-free and in situ alumina-incorporated Pd/SZ catalysts. Furthermore, steady-state activity tests on the modified dual-catalyst bed with the alumina-incorporated Pd/SZ exhibit the best performance amongst the other binder-incorporated catalysts in the dual-catalyst bed. In-situ incorporation of binder during sol-gel synthesis yielded catalysts with far superior catalytic activity for NO_x reduction than conventional ex-situ binder addition to the catalyst slurry for wash-coating. Time-on-stream experiments show that the alumina-incorporated Pd/SZ catalyst maintains the hydrothermal stability of the binder-free Pd/SZ in the mixed bed. Several parameters such as pH of the binder-incorporated catalyst slurry and calcination temperature of the wash-coat have also been optimized to develop a catalytically active wash-coat and its adhesivity and uniformity were tested using ultrasonication, cyclic thermal shock and SEM imaging.

1. Introduction

The highly efficient natural gas-fired lean-burn engines have cleaner engine exhausts as compared to their traditional-stoichiometric counterparts [1]. However, these lean-burn engines still contain considerable levels of pollutants such as nitrogen oxides (NO_x), unburned hydrocarbons (CH_x) and carbon monoxide along with water vapor in their engine exhaust streams. Particularly, NO_x emissions are of great concern as they are responsible for acid rain, smog and formation of ground level ozone. Environmental regulations on permissible limits of emission of nitrogen oxides are getting increasingly stringent. Thus, the development of an efficient aftertreatment system for reduction of NO_x emissions under lean burn conditions has become imperative [2,3].

Conventional aftertreatment systems for NO_x reduction such as three-way catalysts are ineffective under lean conditions since the catalyst is unable to selectively reduce NO_x in presence of excess oxygen [4]. Ammonia selective catalytic reduction (SCR) is more

* Corresponding author.
E-mail address: Ozkan.1@osu.edu (U.S. Ozkan).

http://dx.doi.org/10.1016/j.apcatb.2016.08.062
0926-3373/

suitable for lean-burn conditions, however, there are many drawbacks associated with it which make it uneconomical for small scale systems. Ammonia SCR requires a complex infrastructure with on-site storage of ammonia, high maintenance costs due to formation of ammonium salts, ammonia slip and external injection of ammonia for NO_x reduction [5,6]. A catalytic reduction system that utilizes the unburned hydrocarbons which are already present in the exhaust stream of lean-burn engines is an attractive option as it not only reduces hydrocarbon emissions, but also eliminates the need for injection of an external reducing agent for NO_x reduction [4,7]. This results in a simpler infrastructure than ammonia SCR and makes it a viable alternative for large scale as well as for small scale systems. Methane, which is abundantly available in natural gas and is fairly inexpensive, is a good candidate as a reductant for NO_x emission control. However, activation of methane and the competitive hydrocarbon combustion reaction in the presence of excess oxygen are the major challenges faced in using methane for NO_x reduction.

We had reported earlier a dual catalyst aftertreatment system for natural gas fuelled stationary emission sources consisting of a physical mixture of a reduction catalyst (palladium supported on sulfated zirconia) and an oxidation catalyst (cobalt oxide on ceria) for NO_x reduction with methane under lean burn conditions [8–10]. This dual catalyst system has three functions: (i) NO oxidation to NO_2 (ii) NO_2 reduction to N_2 (iii) oxidation of unutilized hydrocarbons and CO to CO_2. In this scheme, NO gets oxidized to NO_2 over the oxidation catalyst (CoO_x/CeO_2) [11–15]. This step is important because NO_2 has a stronger oxidizing potential when compared to NO and hence gets reduced more easily. The oxidation catalyst also oxidizes unburned hydrocarbons and CO. On the reduction catalyst (Pd/SZ), the NO_2 gets reduced to N_2.

For practical use of the dual-catalyst aftertreatment scheme, it is crucial to develop a catalytically active washcoat for structured supports such as cordierite ($2MgO{\cdot}2Al_2O_3{\cdot}5SiO_2$) monolith cores. Monolithic reactors can handle high throughput of gases typical of environmental applications without leading to pressure drop issues [16]. Under reaction conditions, the reactant gases flow through the parallel channels of the monolith core and react on the catalytically active phase of the core after which the products exit the core [17].

Various techniques for deposition of catalytic washcoat on monolithic cordierite cores have been discussed [18] and it has been found that for ceramic monoliths, washcoating is the most widely used method of loading the active catalyst phase onto the monolith core [19]. Typically, aftertreatment systems for engines should be capable of handling drastic variations in temperature and large volume of high velocity gases [19,20]. If the washcoat adheres poorly to the monolith core under such conditions, the aftertreatment unit will be irreversibly damaged due to the permanent loss of the active phase of the core [21,22]. In order to improve the adhesive properties of the washcoat, a material known as binder is added to the slurry in addition to the catalytic powder that comprises the active phase of the washcoat.

Commonly used binders for washcoating applications are alumina, silica, boehmite and their precursors. Alumina has been used extensively for three–way catalysts and is the most commonly used binder for environmental applications [16,23]. The washcoat should not only adhere well to the monolith core, but it should also retain the catalytic properties of the original powder. The incorporation of binder to the washcoat might affect the catalytic activity of the washcoat as the properties of reduction catalyst are very sensitive to the parameters of the preparation method. Hence, it is important to choose a binder that does not negatively impact the catalytic activity of the washcoat.

This contribution focuses on the in situ incorporation of the binder during sol-gel synthesis on the catalytic activity of the dual-catalyst system. In this study, as a first step towards preparation of an effective and catalytically active washcoat, the effect of the incorporation of the various binders to the reduction catalyst has been explored. Binders, such as alumina, boehmite, bentonite and silica, have been incorporated into the reduction catalyst during the sol-gel synthesis step. The catalytic activity for NO_x reduction of the resulting dual-catalyst bed has been tested under steady-state reaction conditions. The novel technique of in-situ incorporation of binder during catalyst synthesis has been compared to the conventional method of addition of binder to the catalyst slurry in terms of the catalytic activity. The metal loading on the best-performing binder-incorporated catalyst sample has been optimized. The hydrothermal stability of the modified dual-catalyst bed has been tested under simulated engine-exhaust conditions. X-ray diffraction was conducted to study the effect of the binders on the crystal structure of the catalyst. The acid sites on the reduction catalyst samples were investigated using diffuse reflectance Fourier transform spectroscopy and pyridine as the probe molecule. Pd and Zr paramagnetic species were identified using Electron Paramagnetic Resonance (EPR). The best-performing binder incorporated catalyst was further optimized to develop a catalytically active wash-coat with enhanced adhesive properties tested using ultrasonication, cyclic thermal shock and SEM imaging.

2. Experimental

2.1. Catalyst preparation

The reduction catalyst component of the dual-catalyst bed, palladium on sulfated zirconia (Pd/SZ), was prepared via the "one-pot sol-gel" technique [10]. In this method, palladium acetate, the precursor for palladium, is dissolved in *n*-propanol in a three-necked flask. Zirconium propoxide is added to the solution along with the sulfating agent, sulfuric acid. Acetic acid, the hydrolyzing agent, is then added drop-wise into the flask. The solution is stirred until gelation. The sol-gel medium is dried at 110 °C overnight followed by calcination at 700 °C. A modification to the above mentioned synthesis technique involved the in-situ addition of alumina, boehmite, bentonite or silica, referred to as "binder" here onwards, to the sol-gel medium prior to the gelation step. The amount of binder added into the sol-gel medium was 10% (by weight) of the catalyst. Following addition of binder, the sol-gel medium was stirred until gelation, dried and calcined as per the procedure described for the binder-free catalyst.

For further wash-coat development, the binder-incorporated reduction catalyst was dissolved in water keeping the amount of solids in the solvent (water) at 30%. The pH of the resulting slurry was controlled at 1, 4 or 7 using either nitric acid or ammonium hydroxide solution. The wash-coat was dried at 110 °C and the calcination temperature was optimized to form the "wash-coat powder". In order to load the catalyst onto 400 cpsi cordierite monolith cores with 0.115 mm wall thickness (calculated), the cores were dip-coated three times in the washcoat slurry, with 30 min of drying between each dip. Compressed air was blown gently through the monolith to ensure that the channels are not blocked. The coated cores are dried and calcined as per the optimized parameters for the "wash-coat powder". The oxidation catalyst component of the dual-catalyst bed, cobalt supported on ceria (CoO_x/CeO_2), was synthesized using the wet impregnation technique described by Gawade et al. [24].

2.2. Activity testing

Steady state experiments were carried out using a ¼" stainless steel reactor under simulated engine-exhaust conditions. The feed comprises 180 ppm NO_2, 1737 ppm CH_4, 208 ppm C_2H_6,

Table 1
BET surface area and pore volume of the binder-free and binder-incorporated Pd/SZ samples.

Samples	BET surface area (m^2/g)	Pore volume (cc/g)
Pd/SZ	47	0.12
Pd/SZ (alumina-incorporated)	68	0.17
Pd/SZ (boehmite-incorporated)	46	0.14
Pd/SZ (silica-incorporated)	27	0.12

104 ppm C_3H_8, 10% O_2, 10% H_2O, 650 ppm CO, 6.5% CO_2 and balance helium to maintain the total flow rate at 40 cc/min and a gas hourly space velocity of 32000 h^{-1} (WHSV of 6.45 h^{-1}). The catalyst bed is a physical mixture of the reduction catalyst and the oxidation catalyst in the ratio of 8:1. For all the steady-state activity experiments, the reaction experiments were performed using the dual-catalyst bed with either the binder-free or the binder-incorporated reduction catalyst component and from here on these mixed beds will be referred to by their reduction catalyst component, unless mentioned otherwise. Similar conditions were used to test the activity of the wash-coat powder. In order to study the effect of the wash-coating process on catalytic activity, the wash-coat was also scraped off the monolith core and tested under the above mentioned conditions.

The reactor contains the mixed bed and balance quartz powder to keep the gas hourly space velocity (GHSV) constant. The catalyst bed is held in place in the reactor tube between two quartz wool plugs and the reactor is then placed in a resistively-heated furnace fabricated in our laboratory. The temperature of the catalyst bed is monitored with a K-type thermocouple and controlled with an Omega CS232 temperature controller. For studies on the performance of the dual-catalyst bed in the presence of water vapor, a stream of He is saturated with water vapor by passing it through a water bubbler maintained at a set temperature. The saturated He stream is then introduced into the reactor system with the other feed gases. The product stream from the reactor passes through a Permapure membrane for the removal of water vapor from the stream. The composition of the products is analyzed using an Agilent 3000A micro-gas chromatograph equipped with 0.32 mm molecular sieve and PLOT Q columns and a thermal conductivity detector. The nitrogen oxide species are analyzed using a Thermoscientific 42i–HL chemiluminescence NO-NO_2-NO_x analyzer.

2.3. Catalyst characterization

2.3.1. Surface area and pore volume

Micromeritics accelerated surface area and porosimetry instrument (ASAP 2020) was used to analyze the surface area and pore volume of the reduction catalyst samples. Before analyzing the samples, they were degassed at 140 °C under a vacuum of 2 μmHg overnight to rid them of moisture and other adsorbed gases. The surface area of the catalyst samples was determined using the Brunauer-Emmett-Teller (BET) method while the pore volume of the samples were determined using the Barrett-Joiner-Halenda (BJH) method applied on the N_2 adsorption-desorption isotherm at liquid N_2 temperature.

The BET surface area and pore volume of the binder-free and binder-incorporated samples are shown in Table 1. The samples demonstrated the type IV BET isotherm which is characteristic of such materials [25]. It was observed that the alumina-incorporated Pd/SZ catalyst sample has a surface area of 68 m^2/g and a pore volume of 0.17 cm^3/g, which was the highest when compared to the other binder-incorporated Pd/SZ and binder-free Pd/SZ samples. For the oxidation catalyst, the BET surface area has been reported to be 106 m^2/g in our earlier studies [11].

2.3.2. X-ray diffraction

The X-ray diffraction patterns of the binder-free and binder-incorporated Pd/SZ catalyst samples were acquired using the Bruker D8 advanced X-ray diffractometer equipped with a Cu Kα source. The data was collected between 20° to 45° 2θ range with 0.0133 step-size using an 8 mm slit and LynxEye detector. The crystal phases were identified by using the international center for diffraction data (ICDD) database. ICDD# 81-1546 and ICDD# 37-1484 were used to identify the tetragonal and the monoclinic phases of zirconia respectively. Crystal phase analysis was done on the samples using the method described by Toroya et al. for monoclinic-tetragonal zirconia systems [26]. The effect of the addition of the binder on the fraction of the tetragonal phase of zirconia in the samples was studied using the phase analysis.

2.3.3. Diffuse reflectance infrared Fourier transform spectroscopy (DRIFTS)

DRIFTS experiments were conducted using the Thermo Nicolet 6700 FTIR instrument equipped with a mercury-cadmium-telluride detector and a KBr beam splitter. The detector is kept cool with liquid nitrogen. In order to study the acid sites on the binder-free and the binder-incorporated Pd/SZ catalyst samples, pyridine was used as the probe molecule. Due to the strong adsorption of pyridine, the powder catalyst samples were diluted with KBr. The samples were loaded into an in-situ reaction chamber with ZnSe windows. The sample was pretreated at 450 °C under 10% O_2 for 30 min. Following this, the sample was cooled under helium and background spectra collected at 50 °C intervals until 150 °C. Pyridine was then adsorbed on the samples at 150 °C for 30 min. After flushing the sample with helium to remove the pyridine molecules in the gas phase, sample scans were collected from 150 °C to 450 °C at 50 °C intervals.

2.3.4. Electron paramagnetic resonance (EPR)

The paramagnetic species of the binder-free and alumina-incorporated Pd/SZ samples were investigated using the Bruker EMXplus spectrometer. The spectrometer was operated in the X-band at 9.43 GHz with 100 kHz field modulation and 10 G modulation amplitude for both samples. The EPR spectra were first recorded at room temperature (300 K). The samples were then cooled to 100 K using a cryostat with liquid nitrogen and the EPR spectra were recorded. The g-values of the spectral peaks were calculated to compare the spectra and identify the species.

2.3.5. Adhesivity test

1" by 1/3" cordierite monolith cores were dip-coated in either the binder-free reduction catalyst slurry or the wash-coat slurry and dried at 110 °C overnight. The dried cores were then calcined at 700 °C at 1 °C/min ramp rate to prevent the formation of any cracks during calcination. The monolith cores were weighed after calcination to note the amount of catalyst or wash-coat that is loaded onto the core. In order to test the adhesiveness of the catalyst or the wash-coat on the cordierite monolith core, the set of monolith cores were subjected to cyclic thermal shocks at 600 °C with air flowing through the monoliths at 700 ml/min. The monolith cores were then dry sonicated followed by wet sonication in water at 40 kHz using Fisher Scientific FS20H sonicator to simulate harsh conditions after which the percentage loss in weight (dry) was noted.

2.3.6. Scanning electron microscopy (SEM)

Surface morphologies of 1" by 1/2" bare cordierite monolith and wash-coated monolith cores were studied using FEI Nova NanoSEM 400 scanning electron microscope equipped with a field emission

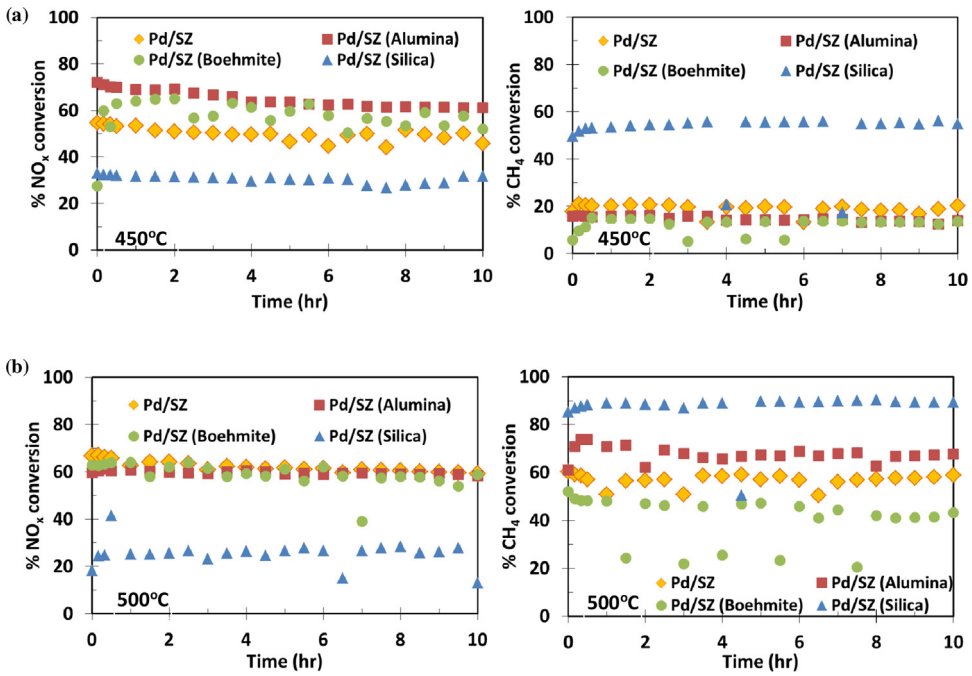

Fig. 1. Effect of different binders on Pd/SZ catalyst in a mixed bed. NO_x conversions and CH_4 conversions at (a) 450 °C and (b) 500 °C in the presence of water vapor in the feed.
Feed conditions: 180 ppm NO_2, 1737 ppm CH_4, 208 ppm C_2H_6, 104 ppm C_3H_8, 650 ppm CO, 6.5% CO_2, 10% O_2, 10% H_2O, GHSV 32000 h^{-1}.

gun (FEG) at 5 kV. The samples were prepared as follows: the bare monolith core was cleaned by sonicating the core in a 1:1 solution of ethanol to water for 30 min followed by sonication in deionized water for an additional hour. The bare monolith core was then dried at 110 °C and calcined at 700 °C for 2 h using a ramp rate of 1 °C/min. The wash-coated monolith core was coated in two cycles of triple dip-coating with drying at 110 °C between dippings, followed by calcination at 700 °C between cycles to increase the loading of the wash-coat. The cross-sectional as well as the side views of the samples were examined using SEM at different magnifications for comparison between samples.

3. Results and discussion

3.1. Effect of the sol-gel incorporated binder

Previously we have demonstrated the hydrothermal stability of the dual-catalyst bed under simulated lean-burn engine exhaust conditions [12]. As a first step towards selection of a suitable binder, the binder-free and the binder-incorporated Pd/SZ catalysts have been tested under the same feed conditions to ensure that addition of binder to the reduction catalyst does not deteriorate its catalytic activity and consequently, impact the performance of the dual-catalyst bed. Equal quantities of commonly used binders such as alumina, boehmite, bentonite or silica were incorporated into the reduction catalyst during the sol-gel synthesis process and the catalytic activity of the resulting reduction catalyst was tested as part of the dual-catalyst bed. For the alumina, boehmite or silica incorporated Pd/SZ catalysts, CO, C_2H_6 and C_3H_8 are completely oxidized under these conditions. NO_2 conversions were over 80% for both reaction temperatures and for all catalysts (not shown). Fig. 1 compares the results from these steady state activity experiments for up to 10 h. We observe that at 450 °C, the alumina-incorporated Pd/SZ and the boehmite-incorporated Pd/SZ significantly improve the water tolerance of the dual-catalyst bed and this is evidenced from the comparison of the catalytic activity of the mixed beds in terms of their NO_x conversions. However, the activity of the alumina-incorporated Pd/SZ containing dual-catalyst bed demonstrates the most stable activity for NO_x reduction with NO_x conversions of 60%. The bentonite-incorporated Pd/SZ (not shown) performed poorly with less than 20% NO_x conversions and less than 5% CH_4 conversions and was not investigated further. At 500 °C, the binder-free Pd/SZ, alumina-incorporated Pd/SZ and boehmite-incorporated Pd/SZ demonstrate comparable activity at 60% NO_x conversion. However, the alumina-incorporated Pd/SZ shows much higher CH_4 conversions of 70% than the binder-free Pd/SZ and the boehmite-incorporated Pd/SZ with CH_4 conversions at 60% and 40% respectively. For both the reaction temperatures, the silica-incorporated Pd/SZ exhibits low conversions for NO_x and high CH_4 conversions. Especially, at the higher reaction temperature of 500 °C, CH_4 conversions are over 90%, leading to not enough hydrocarbons being available for NO_x reduction. Thus, overall, the alumina-incorporated Pd/SZ containing dual-catalyst bed is the best performing mixed bed and demonstrates improved water tolerance in terms of both NO_x conversion as well as CH_4 conversion.

Zalewski et al. studied the effect of addition of binders such as alumina and silica to sulfated zirconia and reported a stronger interaction between alumina and sulfated zirconia due to its acidic nature [27]. Research has also shown that for low Pd loadings on acidic supports, the Pd stabilizes in its active Pd^{2+} cationic phase [28,29] which favors NO_x reduction. Furthermore, the formation of PdO clusters on Pd supported on silica has been reported by researchers [28]. Our earlier studies [30] suggest that direct combustion of methane is favored over the oxidic phase of Pd. In order to examine the effect of the addition of binder to the oxidation state of Pd, we have performed further investigations using X-ray absorption near edge spectroscopy (XANES) and X-ray photoelectron spectroscopy (XPS). Due to low Pd loading and also because of the Pd 3d region overlapping with Zr 3p region, the results were inconclusive and have not been included in this publication. However, from studies reported in the literature, we hypothesize possible reasons for the observations of our activity results. We envision that in the case of the alumina-incorporated Pd/SZ, due to the effect of the strong interaction between alumina and the

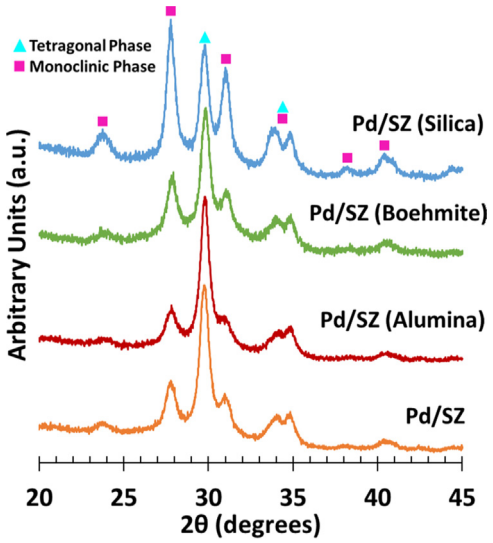

Fig. 2. XRD pattern of binder-free and binder-incorporated Pd/SZ catalysts after calcination at 700 °C.

support on the acidic properties of the sulfated zirconia, Pd is stabilized in its active cationic phase for NO_x reduction whereas in the case of the silica-incorporated Pd/SZ catalyst, PdO clusters formed promote direct methane oxidation rather than NO_x reduction. This may offer a possible explanation for the observed differences in the catalytic performance of the dual-catalyst beds.

3.2. X-ray diffraction (XRD)

The crystal phase of zirconia has been found to significantly affect the activity of the catalyst [27,31,32]. XRD patterns were acquired over the binder-free and binder-incorporated Pd/SZ samples to study the effect of the binder addition to the Pd/SZ samples. The resulting diffractograms in Fig. 2 show that the structure of the catalyst is affected by the type of binder added to the catalyst during its synthesis. The tetragonal as well as the monoclinic phases of zirconia have been identified from the XRD patterns using the ICDD database. Although the monoclinic phase of zirconia is thermodynamically stable at room temperature and the tetragonal phase of zirconia is stable above 1150 °C [25], after calcination of these samples, metastable tetragonal zirconia is observed at room temperature. Studies by Garvie suggest that the formation of metastable tetragonal zirconia is due its lower surface energy when compared to the monoclinic form and that below the critical crystal size of 300 Å, the former is more likely to form [33]. For the binder-free Pd/SZ samples, the formation of the metastable tetragonal phase of zirconia can be attributed to the stabilizing effect of the sulfate groups on the tetragonal zirconia phase by delaying the tetragonal to monoclinic zirconia transformation [25,27,34,35]. For the binder-incorporated Pd/SZ samples, in addition to the stabilizing effect of the sulfates, the presence of the binder may aid in further stabilization of the metastable tetragonal zirconia phase. Addition of binders to Pd/SZ may inhibit crystal growth, thus stabilizing the tetragonal phase of zirconia [27,36,37]. In Fig. 3, the crystal phase analysis after calcination at 700 °C, demonstrates that addition of alumina or boehmite to Pd/SZ stabilizes the metastable tetragonal phase. However, in the case of incorporation of silica to the Pd/SZ catalyst, we observe that the monoclinic phase of zirconia is more dominant in the final catalyst. This could be due to the Si^{4+} ions being smaller than the Zr^{4+} ions [38] resulting in comparatively lower lattice strains than when alumina is added to the support. As a result of this, the tetragonal to monoclinic transformation of zirconia could occur at a lower critical crystal size for the silica-incorporated Pd/SZ samples.

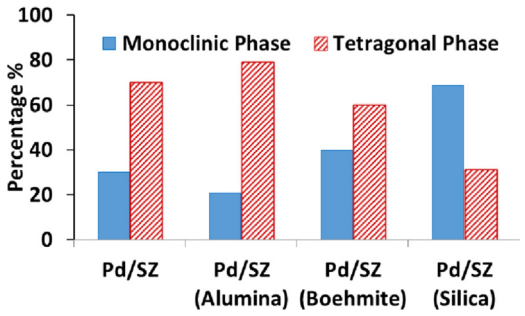

Fig. 3. Crystal phase compositions of binder-free and binder-incorporated Pd/SZ catalysts after calcination at 700 °C.

3.3. Diffuse reflectance infrared Fourier transform spectroscopy (DRIFTS)

Acidity of the support has been found to play an important role in stabilizing the Pd in its active phase on the support for NO_x reduction. In order to study the effect of addition of binders to Pd/SZ on the acidic properties of the resulting catalyst samples, DRIFTS studies were conducted using pyridine as a probe molecule. The IR bands of the pyridine temperature-programmed desorption behavior with respect to temperature are shown in Fig. 4. Fig. 4(a) shows the IR spectra for Pd/SZ in which the ring-stretching region of pyridine is composed of bands signifying physisorbed pyridine, pyridine coordinatively bonded to Lewis acid sites, protonated pyridine indicating Brønsted acid sites, and the interaction between pyridine and surface sulfate groups. Although the adsorption temperature of pyridine is higher than its boiling point temperature, ν_{8a} mode of vibrations associated with the physisorbed pyridine was observed at 1587 cm^{-1}. The presence of this peak can be related to the re-adsorption of desorbed pyridine species. Other modes of ring-stretching vibrations (ν_{8b}, ν_{19a}, and ν_{19b}) corresponding to physisorbed pyridine were not observed [39,40]. It is possible that due to domination by strong overlapping peaks, the peaks corresponding to ν_{8b}, ν_{19a}, and ν_{19b} may be hidden. The peaks at 1605 cm^{-1}, 1572 cm^{-1}, 1487 cm^{-1}, and 1448 cm^{-1} in Fig. 4(a) correspond to Lewis acid sites [39–41]. Presence of 1532 cm^{-1} IR band can be attributed to pyridinium cations [39,40,42,43]. Furthermore, it can be seen that as temperature increases, the peak intensities of the bands associated with Lewis acid sites are decreasing, thus, indicating pyridine desorption from these sites with increase in temperature. Due to the interaction of pyridine with surface sulfate groups, a negative band was observed at 1388 cm^{-1} and it is attributed to the presence of asymmetric surface S=O groups [9,15].

The DRIFTS spectra for the alumina incorporated Pd/SZ, boehmite incorporated Pd/SZ, and silica incorporated Pd/SZ are shown in Fig. 4(b)–(d), respectively. The 1605 cm^{-1}, 1487 cm^{-1}, and 1448 cm^{-1} bands corresponding to Lewis acid sites become more dominant for the binder-incorporated samples. In addition to the Lewis acid sites, several negative bands were observed at 1635 cm^{-1}, 1558 cm^{-1}, 1533 cm^{-1}, and 1483 cm^{-1} which have been reported to be a result of pyridinium cation interaction with Brønsted acid sites [39,40,42–45]. Billingham et al. also observed such a behavior and the decrease in intensity of the peaks was related to hydrogen bond formation of pyridine to the pyridinium cation [43]. While the 1635 cm^{-1} band can also refer to the bending mode ν_{HOH} of coordinated water [46,47], the absence of a strong band due to physisorbed and coordinated water in the high wavenumber region (not shown) may reduce this possibility. Removal of the water from the surface of the catalyst due to

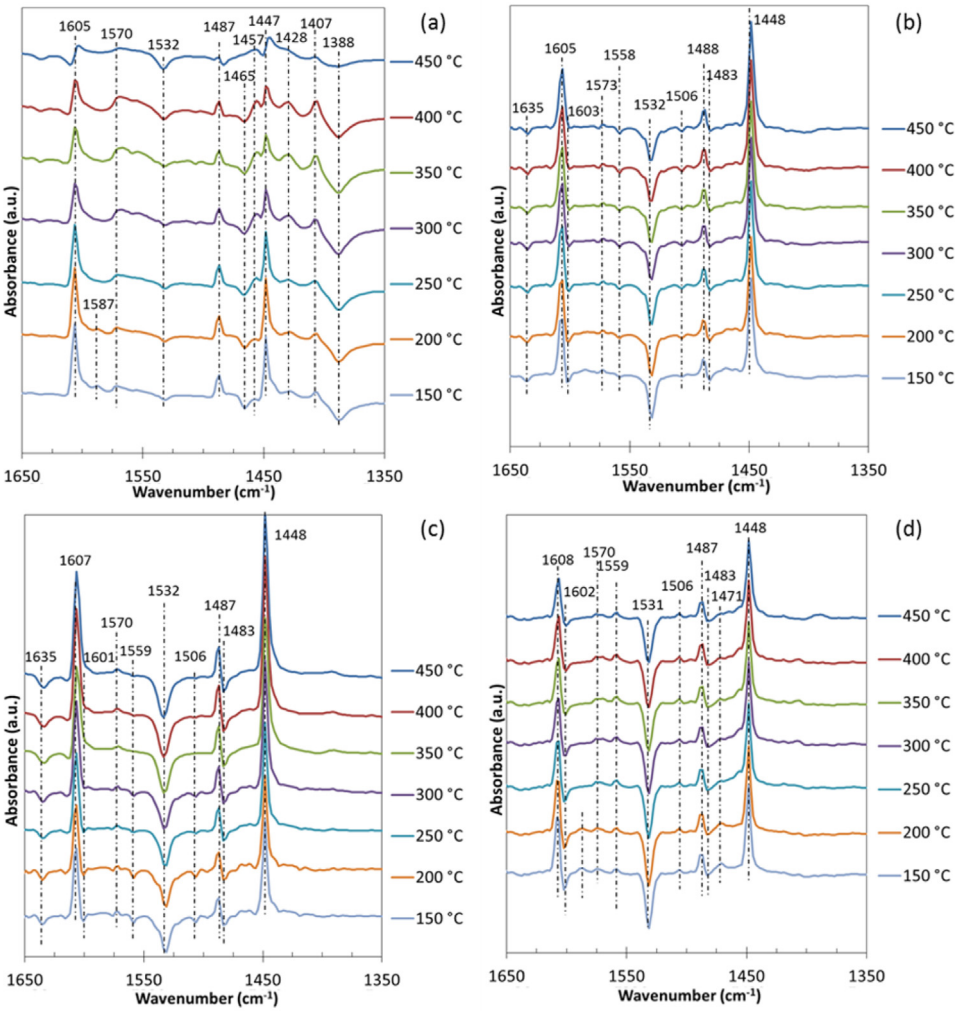

Fig. 4. In-situ DRIFTS spectra of the ring-stretching region during pyridine desorption with respect to temperature. (a) binder-free Pd/SZ (b) Alumina binder- incorporated catalyst, (c) Boehmite binder- incorporated catalyst (d) Silica binder- incorporated catalyst.

oxidative pretreatment at 450 °C may also explain the absence of a strong band in the high wavenumber region. However, the co-existence of peaks at 1635 cm^{-1} and 1532 cm^{-1} suggests that these peaks are most likely due to the pyridinium cations [41], rather than the bending mode of coordinated water. Although these Brønsted acid sites grow slightly weaker with increase in temperature, Lewis and Brønsted acid sites are observed at all the temperatures examined. Fig. 4 shows that addition of binder to Pd/SZ enhances the strength of the Lewis acid sites which is indicated by the strong interaction of these Lewis acid sites with pyridine since their intensities remain almost unchanged as the temperature is increased. Moreover, binder incorporation to Pd/SZ is observed to favor the formation of Brønsted acid sites. Addition of binder also affects the properties of surface sulfur groups. The negative peak at 1388 cm^{-1} showing the asymmetric stretching of S=O is absent in the binder-incorporated samples which may indicate the absence of interaction between pyridine and the surface sulfate species. Thus, this may signify that the sulfate groups on the binder-incorporated samples have a stronger interaction with pyridine when compared to those on the binder-free Pd/SZ sample. Specifically for the alumina-incorporated samples, strong interaction between alumina and the sulfate groups may have a stabilizing effect on the sulfate groups [48].

The tetragonal phase of zirconia has been associated with Lewis acidity and with being more active than the monoclinic zirconia phase for acid-catalyzed reactions [27,32,49]. For DeNO$_x$ catalysis, NO$_x$ conversions on tetragonal zirconia supports have been reported to be higher than that on monoclinic zirconia supports. Furthermore, on tetragonal zirconia, both NO$_x$ reduction and methane oxidation reactions are favored whereas, the monoclinic zirconia support favors methane combustion [50]. For the binder-free, alumina-incorporated Pd/SZ and boehmite-incorporated Pd/SZ containing mixed beds, percentage of tetragonal phase of zirconia is comparatively higher, and under wet conditions, due to rehydration, some of the Lewis acid sites may transform into Brønsted acid sites [51] thus, stabilizing the Pd in its active phase and providing a possible explanation for the higher NO$_x$ conversions observed under reaction conditions.

3.4. Electron paramagnetic resonance (EPR)

The state of palladium plays a crucial role in NO$_x$ reduction under excess oxygen conditions. PdO clusters formed on non-acidic supports favor methane combustion while Pd based on acidic supports was found to be in a cationic Pd form which was active for NO$_x$ reduction [28,52]. Formation of Pd^{n+} cationic species other than Pd^{2+} such as Pd^{+} and Pd^{3+} have also been reported on acidic supports [52]. Sulfated zirconia, being an acidic support, is likely to stabilize palladium in its active phase for reduction of NO$_x$. Pd^{2+} cations, however, are diamagnetic in nature and cannot be observed

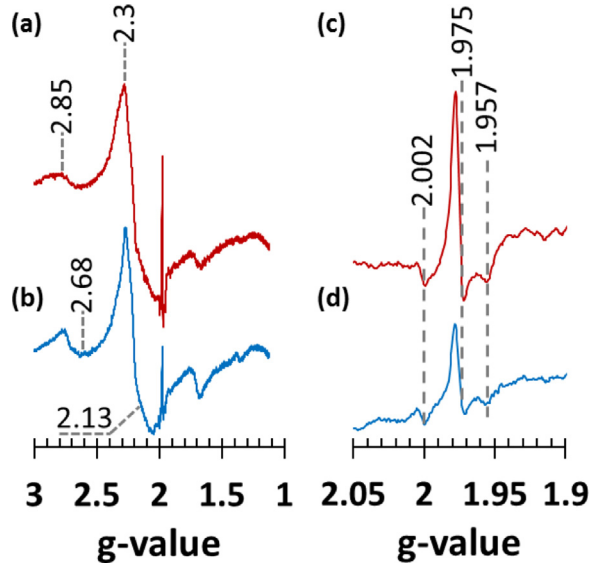

Fig. 5. Electron paramagnetic resonance at 300 K on (a) sol-gel alumina incorporated 0.3% Pd/SZ, (b) binder-free 0.3% Pd/SZ with focus on region 2.05–1.9 for (c) sol-gel alumina incorporated 0.3% Pd/SZ and (d) binder-free 0.3% Pd/SZ.

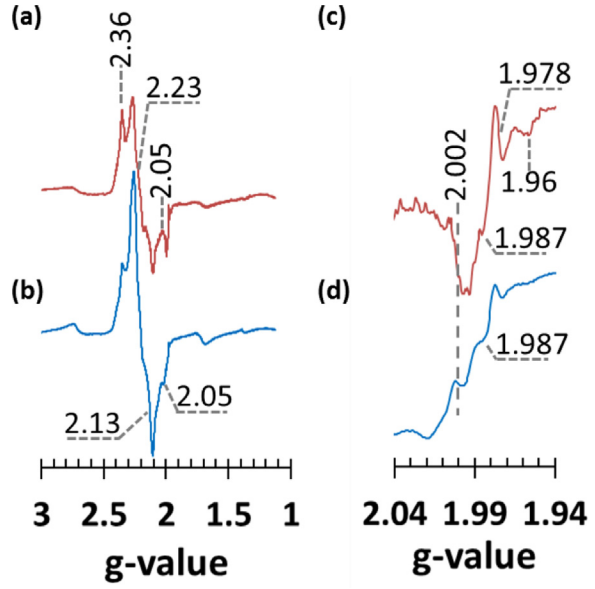

Fig. 6. Electron paramagnetic resonance at 100 K on (a) sol-gel alumina incorporated 0.3% Pd/SZ, (b) binder-free 0.3% Pd/SZ with focus on region 2.04–1.94 for (c) sol-gel alumina incorporated 0.3% Pd/SZ and (d) binder-free 0.3% Pd/SZ.

using EPR; but, Pd^{+} and Pd^{3+} cations being paramagnetic species, are detectable by EPR [53,54]. Furthermore, we can also gain additional understanding about the sulfated zirconia support since only the paramagnetic Zr^{3+} can be observed using EPR while the Zr^{4+} species being diamagnetic cannot be detected. EPR technique can thus provide valuable insights into the state of Pd as well as Zr in the sulfated zirconia support.

Figs. 5 and 6 display the first-derivative of the absorption spectra of the binder-free Pd/SZ and the alumina-binder incorporated Pd/SZ samples using EPR. The g-values of the peaks are calculated to enable species identification. The EPR spectra at 300 K, shown in Fig. 5(a) and (b) reveals $g_{\|}$ and $g_{\perp}$ values of 2.3 and 2.13 respectively which correspond to Pd^{+} species in the samples [55]. In addition, $g_{\|}$ −values at 2.85 and 2.68 with corresponding $g_{\perp}$-values at ~2.10 also indicate the presence of Pd^{+} cations [56]. Pd^{+} cations observed in low-loading Pd catalysts on acidic supports are typically formed by combination of Pd^{2+} species with Pd^{0} or by reduction of the Pd^{2+} cations [54,57].

Fig. 5(c) and (d) focus on the region with g-values between 2.05 and 1.9 for the samples at 300 K. The $g_{\perp}$ and $g_{\|}$ −values observed at 1.975 and ~1.96 indicate the presence of Zr^{3+} paramagnetic species [58]. A high degree of crystallinity is evident from the low anisotropy (Δg ~0.0018) associated with the Zr^{3+} spectra for both samples. The $g_{\perp}$ and $g_{\|}$ −values are less than g_e (2.002), showing d^1 state of Zr^{3+}. It has been suggested that for an ion in the d^1 state, the $g_{\|} < g_{\perp}$ condition may indicate that the ion has octahedral co-ordination with a tetrahedral distortion [59]. The d^1 state of Zr^{3+} also makes the ions sensitive to its oxygen vacancy coordination environment thus enabling change in oxidation state [60,61]. Sulfate decomposition and loss of water during calcination of the samples under oxidizing conditions may lead to the formation of Zr^{3+} ions and oxygen vacancies [58,61,62]. Metastable tetragonal zirconia phase is favored by the presence of lattice defects (oxygen vacancies) around Zr atoms [60,63]. Thus, the presence of Zr^{3+} ions and oxygen vacancies in the catalyst samples contributes to stabilizing zirconia primarily in its tetragonal phase as is evidenced by the XRD experiments discussed earlier.

The alumina-incorporated and binder-free Pd/SZ samples were cooled to 100 K and their EPR spectra are shown in Fig. 6(a) and (b). At 300 K, the broad peak at $g_{\|}$ −value of 2.3 shown in Fig. 5(a) and (b), has hidden features which are revealed when the samples are cooled to 100 K. In Fig. 6(a) and (b), the aforementioned broad peak is resolved into two sharper peaks at 100 K with $g_{\|}$ −value of 2.36 and $g_{\perp}$ −value of 2.13 indicating the presence of Pd^{+} cations and g_{iso} −value of 2.23 suggesting the presence of Pd^{3+} ions [64,65]. High temperature thermal treatment of the low-loading Pd catalyst in an oxidizing environment or interaction of Pd^{2+} cations with water may result in the transformation of some of the Pd^{2+} cations to Pd^{3+} on the catalyst samples [57]. Additionally, the formation of a Pd^{2+}-O^{2-} complex due to molecularly adsorbed O_2 or H_2O on Pd^{+} cations is indicated by the $g_{\perp}$ −value of 2.05 and $g_{\|}$ −value of 1.98 ($g_{\|}$ −value shown in Fig. 6(c) and (d)) [66]. Fig. 6(c) and (d) focus on the EPR spectra of the samples at 100 K between g-values of 2.04-1.94. The presence of Zr^{3+} ions is indicated by $g_{\perp}$ −value of 1.978 and $g_{\|}$ −value of 1.96 in both samples. However, the peak at g_e (2.002) is more intense in the alumina-incorporated Pd/SZ sample and may be attributed in part to Al interaction with oxygen vacancies resulting in free electrons being trapped in these vacancies. Praserthdam and co-workers have also reported improved stabilization of electrons in oxygen vacancies due to Al doping in zirconia [67].

Thus, ESR spectra have revealed paramagnetic Pd^{+} and Pd^{3+} centers formed due to catalyst synthesis parameters or partial transformation of Pd^{2+} cations. The cationic Pd state on acidic supports like sulfated zirconia is crucial for favoring the NO_x reduction reaction over the competitive methane oxidation reaction under excess oxygen conditions. Moreover, in addition to the stabilizing effect of dopants such as sulfates in the case of Pd/SZ or both sulfates and alumina in the case of alumina-incorporated Pd/SZ sample on the tetragonal phase of zirconia, the presence of Zr^{3+} cations with oxygen vacancies also plays an important role in the formation and stability of tetragonal zirconia phase. The possible interaction of Al with oxygen vacancies in the catalyst may result from the sol-gel incorporation of alumina to Pd/SZ and may even indicate the formation of a ZrO_2-Al_2O_3 binary mixture or a solid solution.

3.5. *Effect of binder incorporation method*

To examine the effect of the binder incorporation method, we have also conducted experiments using two different reduction catalysts in the mixed bed, namely Pd/SZ with in-situ binder incor-

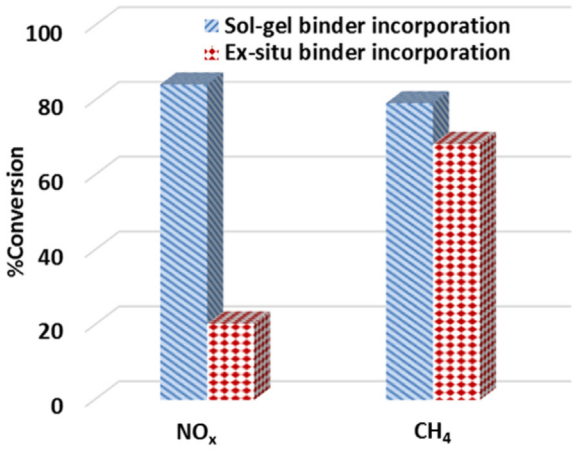

Fig. 7. Comparison between in-situ (during sol-gel) and ex-situ binder incorporation to Pd/SZ. Data collected in the mixed bed at 450 °C. Feed conditions: 180 ppm NO_2, 1737 ppm CH_4, 208 ppm C_2H_6, 104 ppm C_3H_8, 650 ppm CO, 6.5% CO_2, 10% O_2, GHSV 32000 h^{-1}.

poration and Pd/SZ with ex-situ binder incorporation. In the former, the binder was incorporated in situ during the sol-gel synthesis; while, in the latter sample, the binder was added ex situ in a slurry of Pd/SZ and water, following which it was dried, calcined and tested. In both cases, the binder used was alumina. Fig. 7 shows a comparison of the two binder incorporation methods. The sample prepared with in-situ binder incorporation exhibits much higher activity, with NO_x conversion levels of 80%, while the ex-situ binder incorporation results in a in a much lower conversion (20%). The CH_4 conversion for the sample prepared with in-situ binder incorporation is also higher than that of the sample prepared by ex-situ binder incorporation, but the difference is not as pronounced. This result is significant in demonstrating that sol-gel incorporation of the binder provides a superior catalyst. In situ addition of binder during sol-gel synthesis may result in the stronger Al-support interaction and consequently affect the catalytic activity for NO_x reduction under lean conditions.

3.6. Effect of Pd loading

The Pd loading on the alumina-incorporated Pd/SZ catalyst has been optimized by testing the performance of the mixed beds with the reduction catalyst component having 0.1%, 0.3% or 0.5% Pd metal loading. As shown in Fig. 8, we observe that the total NO_x conversion is highest at a loading level of 0.3% at both temperatures. The methane conversions, on the other hand, appear to improve with increasing Pd loading on the reduction catalyst component of the mixed bed at both 450 °C and 500 °C. While the methane conversion for the catalyst bed with the 0.1% Pd/SZ, increases from 5% conversion to 20% with increase in reaction temperature, for the bed with the 0.3% Pd/SZ and 0.5% Pd/SZ, the methane conversions increase from 20% to 70% and 25% to 80%, respectively. Higher Pd loading (0.5%) favors methane oxidation resulting in depletion of the reducing agent for the NO_x reduction reaction. Higher Pd loading may also result in the formation of PdO clusters which would lead to complete oxidation (combustion) of methane. For the lower Pd loading (0.1%), methane activation may be too low hindering the reduction of NO_x since the overall NO_x reduction reaction is dependent on methane activation.

For the middle Pd loading (0.3%), the Pd is likely stabilized in its active cationic form and the synergistic effect between the reduction and the oxidation catalyst is optimum for NO_x reduction under lean condition [68,69]. These results are also consistent with studies conducted on the Pd/SZ catalyst wherein a higher Pd metal loading has been found to increase methane conversions, mostly due to direct oxidation of CH_4 with molecular O_2 [8]. Thus, overall, in terms of both the NO_x conversions and the methane conversions, the 0.3% Pd loading on the reduction catalyst can be considered to give the optimum performance of the dual-catalyst bed.

3.7. Hydrothermal stability

Time-on-stream experiments were conducted for over 40 h on the alumina-incorporated Pd/SZ containing dual-catalyst bed to test how it compares with the hydrothermal stability test previously conducted on the binder-free Pd/SZ containing mixed bed at 450 °C [12]. The results from this experiment are presented in Fig. 9. We observe that the mixed bed containing the alumina-incorporated Pd/SZ, after an initial drop in activity, demonstrates good hydrothermal stability, maintaining the same NO_x conversion level between 20 and 40 h. Also, addition of the alumina binder to Pd/SZ is seen to improve the catalytic activity in terms of NO_x conversions. These results are significant in showing that sol-gel incorporation of the alumina offers a promising technique for further development of a catalytically active washcoat.

3.8. Wash-coat development

In order to load the powdered catalyst onto a cordierite monolith core, we have developed a catalytically active washcoat by optimizing parameters such as the pH of the slurry and the calcination temperature of the dried wash-coat. The steps involved in preparation of the wash-coat from the insitu alumina-binder incorporated Pd/SZ strongly affected the catalytic activity of the resulting wash-coat. The activity of the wash-coat as part of the dual-catalyst aftertreatment system was tested to investigate the effect of the above mentioned wash-coating parameters. The cordierite core was then coated with the best performing wash-coat followed by scraping off the wash-coat from the core to study its activity in powder form using the fixed bed reactor. The adhesivity of the wash-coat to the monolith core was also tested using cyclic thermal shock treatments and ultrasonication. The results of the effect of the wash-coating parameters on catalytic activity of the wash-coat with an insight into the uniformity of the best −performing wash-coat on the monolith core using SEM imaging and the adhesivity tests have been discussed in this section.

3.8.1. Effect of pH

The effect of pH of the catalyst slurry on the catalytic activity for NO_x was studied using simulated engine exhaust conditions. The slurry was dried and tested as part of the dual-catalyst bed under reaction conditions for 4 h. In this section, the dual-catalyst bed will be referred to by the pH that the alumina-incorporated Pd/SZ slurry was controlled at. Fig. 10(a) represents the NO_x conversion data at reaction temperatures of 450 °C and 500 °C. At 450 °C, the NO_x conversions of pH 1 and pH 7 are comparable at close to 40% and that for pH 4 is at 20% and no significant change in the conversions with increase in temperature to 500 °C was observed. The CH_4 conversions shown in Fig. 10(b) demonstrates that as the reaction temperature is increased from 450 °C to 500 °C, for pH 1, the CH_4 conversion improved from 40% at 450 °C to ~80% at 500 °C while that for pH 4 remained the same and for pH 7 increased to over 30% conversion. Thus, it was observed that at reaction temperatures of 450 °C and 500 °C, pH 1 demonstrated better activity for NO_x as well as CH_4 conversions. For further wash-coat development, the alumina-incorporated Pd/SZ slurry was controlled at a pH of 1.

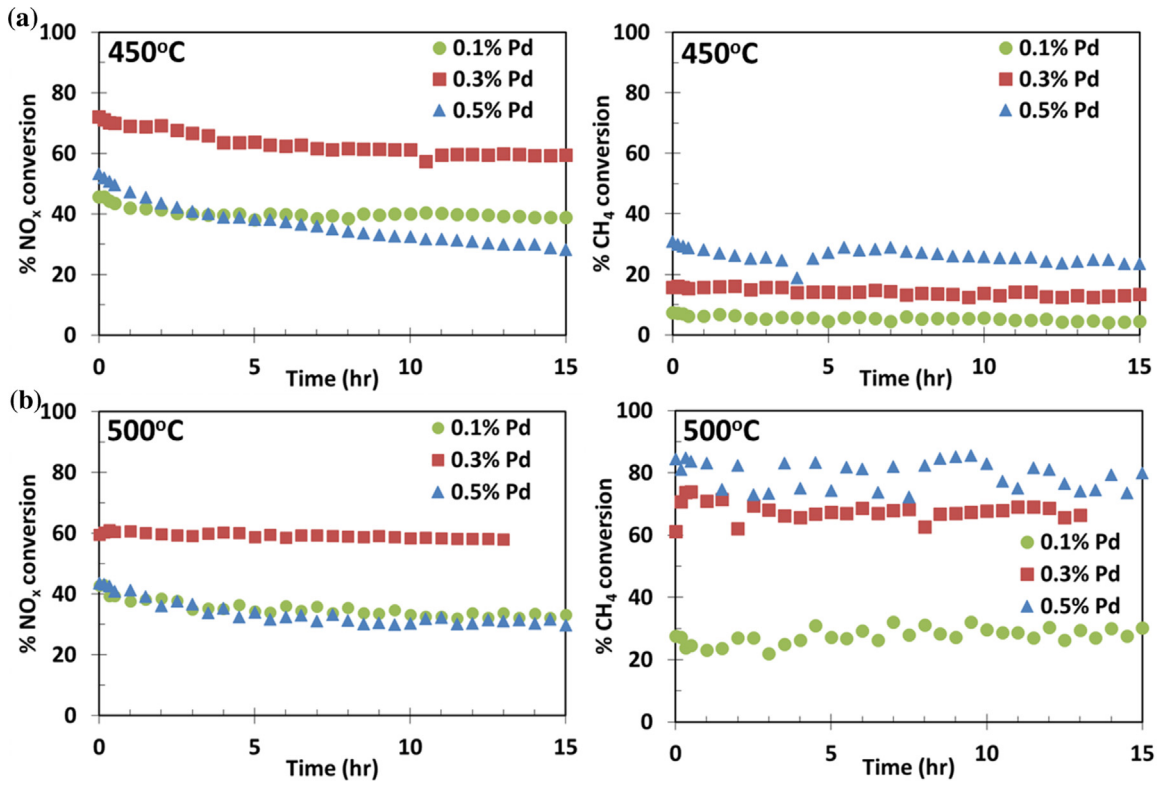

Fig. 8. Effect of palladium loading over a mixed bed containing alumina binder-incorporated PdSZ as reduction catalyst component. NO_x conversions and CH_4 conversions at (a) 450 °C and (b) 500 °C in the presence of water vapor in the feed.
Feed conditions: 180 ppm NO_2, 1737 ppm CH_4, 208 ppm C_2H_6, 104 ppm C_3H_8, 650 ppm CO, 6.5% CO_2, 10% O_2, 10% H_2O, GHSV 32000 h^{-1}.

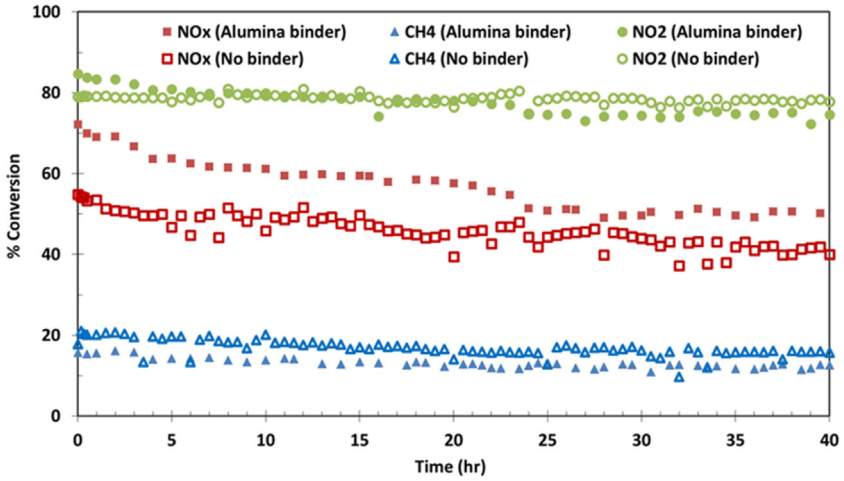

Fig. 9. Hydrothermal stability of alumina incorporated Pd/SZ catalyst at 450 °C in the presence of water vapor in the feed.
Feed conditions: 180 ppm NO_2, 1737 ppm CH_4, 208 ppm C_2H_6, 104 ppm C_3H_8, 650 ppm CO, 6.5% CO_2, 10% O_2, 10% H_2O, GHSV 32000 h^{-1}.

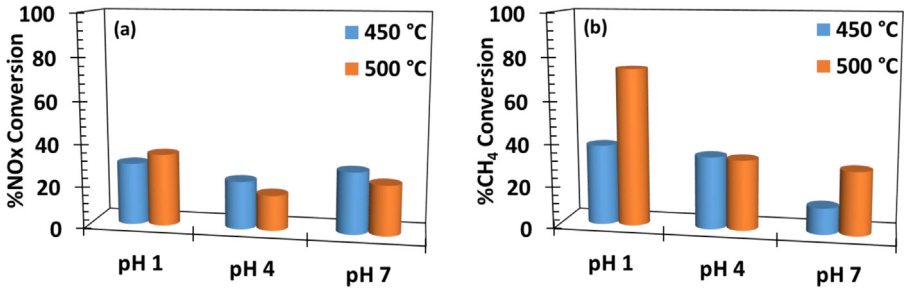

Fig. 10. Effect of pH of Pd/SZ (alumina) containing slurry on the (a) NO_x conversion and (b) CH_4 conversion activity of the dual-catalyst bed at 450 °C and 500 °C.
Feed conditions: 180 ppm NO_2, 1737 ppm CH_4, 208 ppm C_2H_6, 104 ppm C_3H_8, 650 ppm CO, 6.5% CO_2, 10% O_2, 10% H_2O, GHSV 32000 h^{-1}.

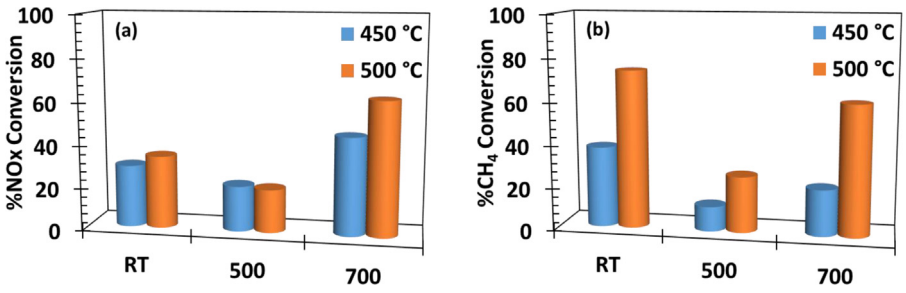

Fig. 11. Effect of calcination temperature of the Pd/SZ (alumina) containing slurry on the (a) NO_x conversion and (b) CH_4 conversion activity of the dual-catalyst bed at 450 °C and 500 °C.
All the slurries at pH 1.
Feed conditions: 180 ppm NO_2, 1737 ppm CH_4, 208 ppm C_2H_6, 104 ppm C_3H_8, 650 ppm CO, 6.5% CO_2, 10% O_2, 10% H_2O, GHSV 32000 h^{-1}.

3.8.2. *Effect of calcination temperature*

Alumina-incorporated Pd/SZ slurry at pH 1 was dried and further processed by calcining at different temperatures to improve its performance. The activity of the uncalcined wash-coat, and wash-coats calcined at 500 °C and 700 °C were tested as part of the dual-catalyst bed under simulated engine exhaust conditions. Fig. 11 displays the comparison between the catalytic activities of the uncalcined wash-coat (RT) with the ones calcined at 500 °C (500) and at 700 °C (700) in the dual-catalyst configuration. As shown in Fig. 11(a), at the reaction temperature of 450 °C, the wash-coat calcined at 700 °C demonstrated higher NO_x conversions at close to 50% when compared to the wash-coat calcined at 500 °C as well as the uncalcined washcoat which were at less than 40% and at 20% respectively. At the reaction temperature of 500 °C, we observed that while the NO_x conversions for the uncalcined wash-coat and wash-coat calcined at 500 °C were similar to those at the reaction temperature of 450 °C, the NO_x conversion for the wash-coat calcined at 700 °C improved to 60%. The CH_4 conversions in Fig. 11(b) showed that with increase in the reaction temperature from 450 °C to 500 °C, an increase in CH_4 conversions was observed for all the samples with ~70%, 60% and 20% for the uncalcined wash-coat, the wash-coat calcined at 700 °C and at 500 °C respectively. Overall, the performance of the alumina-incorporated Pd/SZ slurry with the pH controlled at 1 and calcined at 700 °C demonstrated promising results for use as a wash-coat for the reduction catalyst component of the dual-catalyst bed for NO_x reduction with methane under lean-burn conditions.

3.8.3. *Effect of wash-coating process*

In order to study the effect of the wash-coating process for loading the catalyst onto the cordierite monolith core, the monolith core was dipped in the alumina-incorporated Pd/SZ slurry controlled at a pH of 1. The coated monolith was dried and calcined with a heating ramp of 1 °C/min to 700 °C to prevent the formation of any cracks on the coating. The wash-coat was then scraped off the monolith and tested as part of the dual-catalyst bed under simulated engine exhaust conditions. Fig. 12 shows the result of the activity tests at 450 °C in which we observed that both the NO_x and the CH_4 conversions of the wash-coat powder and the monolith scraping were comparable at 40% and 20%, respectively. These results demonstrated that the coating process did not negatively affect the activity of the wash-coat.

Furthermore, the adhesivity of the wash-coat on the cordierite monolith core was examined by subjecting the wash-coated cordierite core and the binder-free Pd/SZ coated core to thermal shocks by introducing the cores to the heated zone at 600 °C under flowing air followed by sudden cooling under ambient conditions. After ten heating and cooling cycles each, the monolith cores were dry sonicated followed by wet sonication in water for 1 h. The percentage loss in weight for the binder-free sample was 41% while

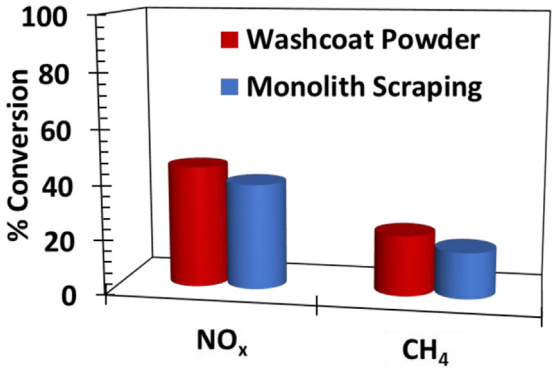

Fig. 12. Comparison between wash-coat and scraped monolith at 450°C in terms of NO_x conversion and CH_4 conversion.
Feed conditions: 180 ppm NO_2, 1737 ppm CH_4, 208 ppm C_2H_6, 104 ppm C_3H_8, 650 ppm CO, 6.5% CO_2, 10% O_2, 10% H_2O, GHSV 32000 h^{-1}.

that for the wash-coated cordierite core was 7%. Thus, in-situ binder addition to the wash-coat significantly enhances the adhesive properties of the coating.

The uniformity of the wash-coat was also examined using SEM and a comparison between the bare monolith core and wash-coated monolith core is presented in Fig. 13 at magnifications of 50×, 250× and 10000×. Fig. 13(a) reveals the cross-section of the skeletal walls of the bare monolith core with the predominantly flat surface topography observed from the side view of the bare monolith. The surface topography of the bare monolith core sharply contrasts the surface morphology of the wash-coated monolith as seen in Fig. 13(b). In this figure, the cross-section of the walls of the monolith core appears to be thicker at the same magnification with a uniform coating of binder-incorporated washcoat on them. The wash-coat on the bare monolith core was found to be ~60 μm in thickness. Furthermore, at a magnification of 10000×, the porosity of the surface due to the coating of the wash-coat was evident. For a 1"x1" core, a maximum loading of 1.05 g was achieved. Thus, a catalytically active wash-coat with superior adhesive properties has been developed using a novel method of in-situ incorporation of binder to the catalyst during the sol-gel process for NO_x reduction under lean-burn conditions.

4. Conclusions

In order to make the dual-catalyst aftertreatment system viable for practical use, the powder catalysts need to be wash-coated onto a cordierite monolith core. Disintegration of the active catalyst phase from the monolith cores is one of the major reasons for irreversible loss of activity for aftertreatment units. Thus, it is important to select a binder that would ensure good adherence of

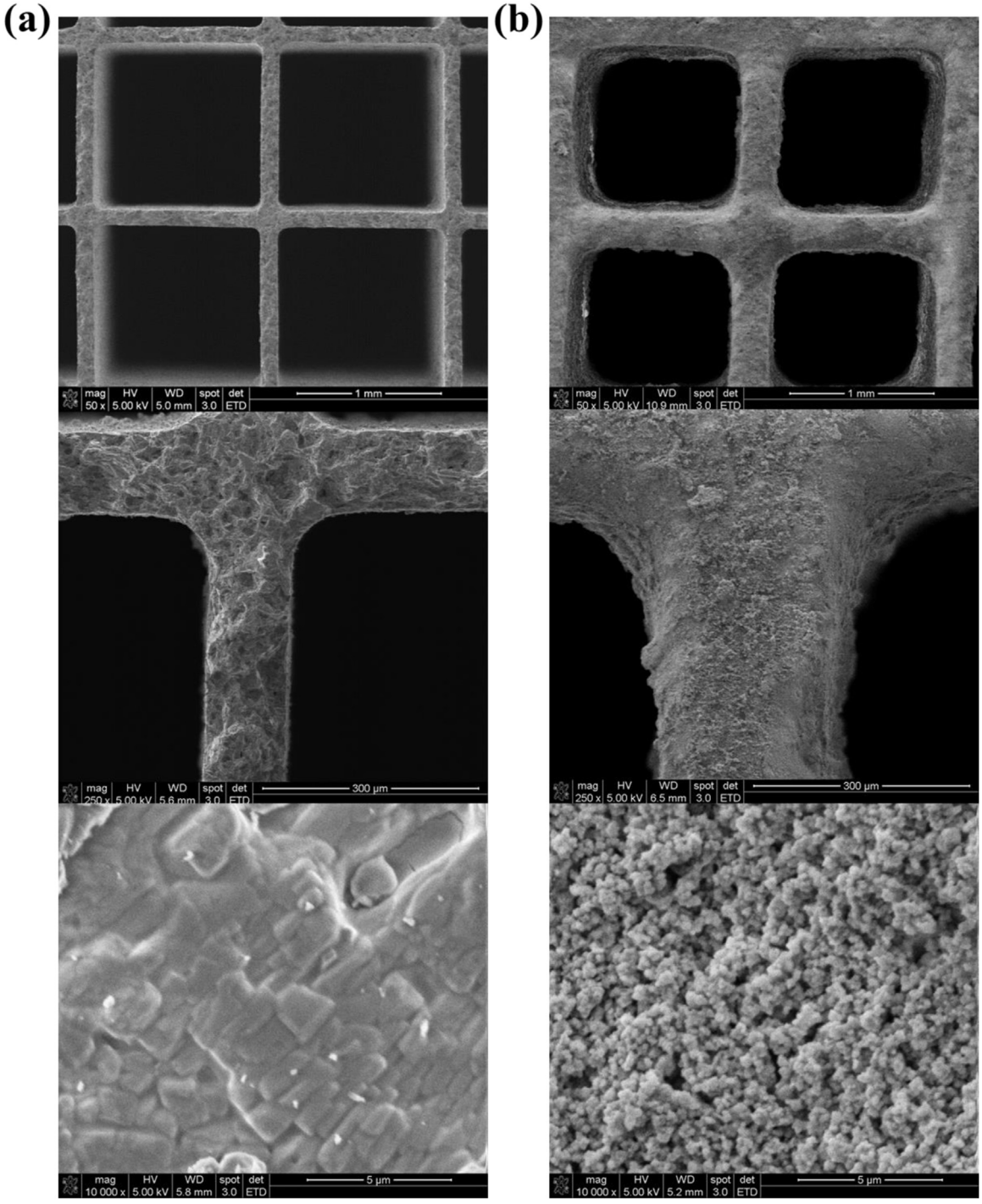

Fig. 13. Comparison between SEM images of (a) Uncoated cordierite core and (b) Wash-coated cordierite core.

the washcoat to the walls of the monolith core and also maintain the catalytic activity of the original powdered catalyst. A novel technique for incorporation of binder to the wash-coat was developed in which the binder was added in situ during sol-gel synthesis of the reduction catalyst. As a first step towards development of an active wash-coat, commonly used binders such as alumina, boehmite, bentonite or silica were incorporated into the reduction catalyst, Pd/SZ.

XRD and DRIFTS studies show that addition of binder to Pd/SZ affects the structural properties as well as the acidic properties of the final catalyst. Incorporation of alumina or boehmite to Pd/SZ during the preparation step led to stabilization of the tetragonal phase of zirconia whereas on addition of silica, the monoclinic zirconia phase was dominant in the resulting catalyst. DRIFTS studies with pyridine as the probe molecule demonstrated that incorporation of binder enhanced the acidic properties of the final catalyst as well as the stability of the sulfate groups on the catalyst. EPR spectroscopy revealed the presence of paramagnetic Pd^{+}, Pd^{3+} and Zr^{3+} species in the binder-free and alumina-binder incorporated Pd/SZ catalysts. These paramagnetic Pd species are likely formed due to partial transformation of Pd^{2+} species on the sulfated zirconia support. The cationic state of Pd on the sulfated zirconia support is crucial for NO_x reduction with methane under excess oxygen conditions. Possible interaction of Al with oxygen vacancies

in the support has also been indicated by the trapped paramagnetic electrons at low temperatures.

Furthermore, steady-state activity tests on the dual-catalyst bed showed that Pd/SZ with in situ alumina binder incorporation as its reduction catalyst component had the most promising performance in terms of catalytic activity for NO_x reduction when compared to the other binder-incorporated Pd/SZ catalysts. Time-on-stream experiments have demonstrated that addition of alumina to Pd/SZ also maintains the hydrothermal stability of the dual-catalyst bed. Moreover, on comparing the effect of the mode of incorporation of binder on the activity for NO_x reduction, in-situ incorporation of alumina binder during sol-gel synthesis of Pd/SZ resulted in a far superior catalyst than ex-situ incorporation of the binder. This was a significant result for further wash-coat development for NO_x reduction.

In order to retain the catalytic activity of the reduction catalyst after it is loaded onto a cordierite monolith core, several parameters such as the pH of the alumina-incorporated Pd/SZ slurry and calcination temperature of the wash-coat were optimized. The best performance of the wash-coat was observed when the pH of the slurry was controlled at 1 and the dried wash-coat was calcined at 700 °C. Adhesivity tests revealed that addition of alumina binder to Pd/SZ also improved the adhesive properties of the wash-coat. Cyclic thermal shock tests followed by sonication on the coated cores resulted in over five times more loss of binder-free coating from the core than the wash-coat developed using in situ binder incorporation.

SEM images also revealed the surface morphology of the wash-coat prepared by the in situ binder incorporation technique. Thus, a wash-coat which is not only catalytically active for NO_x reduction, but also demonstrates excellent adhesive properties has been developed using a novel method of in-situ binder incorporation into the catalyst during sol-gel synthesis.

Acknowledgement

The financial support provided by the US Department of Energy and Caterpillar Inc. is gratefully acknowledged. The authors thank Dr. Ronald Silver of Caterpillar Inc. for his valuable inputs through many detailed discussions. The authors also thank Dr. Gordon Renkes for his assistance in acquiring the EPR data.

References

[1] G.R. Gerber, M.A. Devine, Efficiency, emissions advances keep recip engines in the DG mix, Power 147 (2003) 24–29.
[2] L.R. Raber, EPA's air standards pushing too far, too fast? Chem. Eng. News 75 (1997) 10–18.
[3] R.M. Heck, R.J. Farrauto, Automobile exhaust catalysis, Appl. Catal. A 221 (2001) 443–457.
[4] M. Iwamoto, H. Yahiro, Novel catalytic decomposition and reduction of NO, Catal. Today 22 (1994) 5–18.
[5] M. Iwamoto, H. Hamada, Removal of nitrogen monoxide from exhaust gases through novel catalytic processes, Catal. Today 10 (1991) 57–71.
[6] R.M. Heck, Catalytic abatement of nitrogen oxides-stationary applications, Catal. Today 53 (1999) 519–523.
[7] M.D. Amiridis, T. Zhang, R.J. Farrauto, Selective cataytic reduction of nitric oxide by hydrocarbons, Appl. Catal. B 10 (1996) 203–227.
[8] E.M. Holmgreen, M.M. Yung, U.S. Ozkan, Pd-supported on sulfated monoclinic zirconia for the reduction of NO2 with methane under lean conditions, Catal. Lett. 111 (2006) 19–26.
[9] E.M. Holmgreen, M.M. Yung, U.S. Ozkan, Dual-catalyst aftertreatment of lean-burn natural gas engine exhaust, Appl. Catal. B: Environ. 74 (2007) 73–82.
[10] E.M. Holmgreen, M.M. Yung, U.S. Ozkan, Pd-based sulfated zirconia prepared by a single step sol-gel procedure for lean NOx reduction, J. Mol. Catal. A: Chem. 270 (2007) 101–111.
[11] P. Gawade, A.-M.C. Alexander, R. Clark, U.S. Ozkan, The role of oxidation catalyst in dual-catalyst bed for after-treatment of lean burn natural gas exhaust, Catal. Today 197 (2012) 127–136.
[12] P. Gawade, A.-M.C. Alexander, R. Silver, U.S. Ozkan, Effect of engine exhaust parameters on the hydrothermal stability of hydrocarbon-selective catalytic reduction (SCR) catalysts for lean- burn systems, Energy Fuels 26 (2012) 7084–7091.
[13] M.M. Yung, E.M. Holmgreen, U.S. Ozkan, Cobalt-based catalysts supported on titania and zirconia for the oxidation of nitric oxide to nitrogen dioxide, J. Catal. 247 (2007) 356–367.
[14] B. Mirkelamoglu, M. Liu, U.S. Ozkan, Dual-catalyst aftertreatment of lean-burn engine exhaust, Catal. Today 151 (2010) 386–394.
[15] B. Mirkelamoglu, U.S. Ozkan, Effect of water vapor on the activity and stability of Pd/SZ and Co/ZrO2 in dual-catalyst treatment of simulated exhaust from lean-burn natural gas engines, Appl. Catal. B 96 (2010) 421–433.
[16] P. Avila, M. Montes, E.E. Miró, Monolithic reactors for environmental applications: a review on preparation technologies, Chem. Eng. J. 109 (2005) 11–36.
[17] R.M. Heck, S. Gulati, R.J. Farrauto, The application of monoliths for gas phase catalytic reactions, Chem. Eng. J. 82 (2001) 149–156.
[18] V. Meille, Review on methods to deposit catalysts on structured surfaces, Appl. Cata. A: Gen. 315 (2006) 1–17.
[19] A.V. Boix, E.E. Miró, E.A. Lombardo, J.L.G. Fierro, The inhibiting effect of extra-framework Al on monolithic Co-ZSM5 catalysts used for NOx SCR, Catal. Today 133–135 (2008) 428–434.
[20] A.V. Boix, E.E. Miroí, E.A. Lombardo, R. Mariscal, J.L.G. Fierro, Binder effect upon the catalytic behavior of PtCoZSM5 washcoated on cordierite monoliths, Appl. Cata. A: Gen. 276 (2004) 197–205.
[21] A.V. Boix, J.M. Zamaro, E.A. Lombardo, E.E. Miró, The beneficial effect of silica on the activity and thermal stability of PtCoFerrierite-washcoated cordierite monoliths for the SCR of NOx with CH4, Appl. Catal. B: Environ. 46 (2003) 121–132.
[22] T.A. Nijhuis, A.E.W. Beers, T. Vergunst, I. Hoek, F. Kapteijn, J.A. Moulijn, Preparation of monolithic catalysts (Review), Cat. Rev.—Sci. Eng. 43 (2001) 345–380.
[23] V. Meille, S. Pallier, G.V. Santa Cruz Bustamante, M. Roumanie, J.-P. Reymond, Deposition of gamma Al2O3 layers on structured supports for the design of new catalytic reactors, Appl. Cata. A: Gen. 286 (2005) 232–238.
[24] P. Gawade, B. Bayram, A.-M.C. Alexander, U.S. Ozkan, Preferential oxidation of CO (PROX) over CoOx/CeO2 in hydrogen-rich streams: effect of cobalt loading, Appl. Catal. B: Environ. (2012).
[25] B. Mirkelamoglu, M. Liu, U.S. Ozkan, Dual-catalyst aftertreatment of lean-burn engine exhaust, Catal. Today 151 (2010) 386–394.
[26] H. Toraya, M. Yoshimura, S. Somiya, Calibration curve for quantitative analysis of the monoclinic-tetragonal ZrO2 system by X-ray diffraction, Comm. Am. Ceram. Soc. 67 (1984) C119–C121.
[27] D.J. Zalewski, S. Alerasool, P.K. Doolin, Characterization of catalytically active sulfated zirconia, Catal. Today 53 (1999) 419–432.
[28] A. Ali, W. Alvarez, C.J. Loughran, D.E. Resasco, State of Pd on H-ZSM-5 and other acidic supports during the selective reduction of NO by CH4 studied by EXAFS/XANES, Appl. Catal. B 14 (1997) 13–22.
[29] Y.-H. Chin, A. Pisanu, L. Serventi, W. Alvarez, D.E. Resasco, NO reduction by CH4 in the presence of excess O2 over Pd/sulfated zirconia catalysts, Catal. Today 54 (1999) 419–429.
[30] M.W. Kumthekar, U.S. Ozkan, Nitric oxide reduction with methane over Pd/TiO2 catalysts, J. Catal. 171 (1997) 54–66.
[31] C. Morterra, G. Cerrato, F. Pinna, M. Signoretto, Crystal phase, spectral features, and catalytic activity of sulfate-doped zirconia systems, J. Catal. 157 (1995) 109–123.
[32] R.A. Comelli, C.R. Vera, J.M. Parera, Influence of ZrO2 crystalline structure and sulfate ion concentration on the catalytic activity of So2-4- ZrO2, J. Catal. 151 (1995) 96–101.
[33] R.C. Garvie, The occurrence of metastable tetragonal zirconia as a crystallite size effect, J. Phys. Chem. 69 (1965) 1238–1243.
[34] P. Bautista, M. Faraldos, M. Yates, A. Bahamonde, Influence of sulphate doping on Pd/zirconia based catalysts for the selective catalytic reduction of nitrogen oxides with methane, Appl. Catal. B: Environ. 71 (2007) 254–261.
[35] C.J. Norman, P.A. Goulding, I. McAlpine, Role of anions in the surface area stabilisation of zirconia, Catal. Today (1994) 313–321.
[36] T. Klimova, M.L. Rojas, P. Castillo, R. Cuevas, Characterization of Al2O3-ZrO2 mixed oxide catalytic supports prepared by the sol-gel method, Microporous Mesoporous Mater. 20 (1998) 293–306.
[37] J.-D. Lin, J.-G. Duh, Crystallite size and microstrain of thermally aged low-ceria- and low-yttria-doped zirconia, J. Am. Ceram. Soc. 81 (1998) 853–860.
[38] F.d. Monte, W. Larsen, J.D. Mackenzie, Stabilization of tetragonal ZrO2 in ZrO2-SiO2 binary oxides, J. Am. Ceram. Soc. 83 (2000) 628–634.
[39] M.I. Zaki, M.A. Hasan, F.A. Al-Sagheer, L. Pasupulety, In situ FTIR spectra of pyridine adsorbed on SiO2-Al2O3, TiO2, ZrO2 and CeO2: general considerations for the identification of acid sites on surfaces of finely divided metal oxides, Coll. Surf. A 190 (2001) 261–274.
[40] G. Larsen, S. Raghavan, M. Marquez, E. Lotero, Tungsta supported on zirconia and alumina catalysts: temperature-programmed desorption/reaction of methanol and pyridine DRIFTS studies, Catal. Lett. 37 (1996) 57–62.
[41] G.D. Parfitt, J. Ramsbothaman, C.H. Rochester, An infra-red study of pyridine adsorption on rutile surfaces, Trans. Faraday Soc. 67 (1971) 1500–1506.
[42] B. Li, R.D. Gonzalez, An in situ DRIFTS study of the deactivation and regeneration of sulfated zirconia, Catal. Today 46 (1998) 55–67.
[43] J. Billingham, C. Breen, J. Yarwood, In situ determination of Bronsted/Lewis acidity on cation-exchanged clay mineral surfaces by ATR-IR, Clay Miner. 31 (1996) 513–522.

[44] J.-C. Lavalley, R. Anquetil, J. Czyzniewska, M. Ziolek, Use of pyridine as a probe for the determination by IR spectroscopy, of the Bronsted acid strength of MHNaY zeolites, J. Chem. Soc. Faraday Trans. 92 (1996) 1263–1266.
[45] D. Topaloğlu Yazici, C. Bilgiç, Determining the surface acidic properties of solid catalysts by amine titration using Hammett indicators and FTIR-pyridine adsorption methods, Surf. Interface Anal. 42 (2010) 959–962.
[46] J.W. Ward, A spectroscopic study of the surface of zeolite Y. II. Infrared spectra of structural hydroxyl groups and adsorbed water on alkali, alkaline earth, and rare earth ion-Exchanged zeolites, J. Phys. Chem. 72 (1968) 4211–4223.
[47] A. Sinhamahapatra, N. Sutradhar, M. Ghosh, H.C. Bajaj, A.B. Panda, Mesoporous sulfated zirconia mediated acetalization reactions, Appl. Cata. A: Gen. 402 (2011) 87–93.
[48] P. Canton, R. Olindo, F. Pinna, G. Strukul, P. Riello, M. Meneghetti, G. Cerrato, C. Morterra, A. Benedetti, Alumina-promoted sulfated zirconia system: structure and microstructure characterization, Chem. Mater. 13 (2001) 1634–1641.
[49] W. Stichert, F. Schluth, S. Kuba, H. Knozinger, Monoclinic and tetragonal high surface area sulfated zirconias in burane isomerization: CO adsorption and catalytic results, J. Catal. 198 (2001) 277–285.
[50] A. Bahamonde, F. Mohino, M. Rebollar, M. Yates, P. Avila, S. Mendioroz, Pillared clay and zirconia-based monolithic catalysts for selective catalytic reduction of nitric oxide by methane, Catal. Today 69 (2001) 233–239.
[51] C. Morterra, G. Cerrato, V. Bolis, Lewis and Bronsted acidity at the surface of sulfate-doped ZrO2 catalysts, Catal. Today 17 (1993) 505–515.
[52] A. Ali, Y.-H. Chin, D.E. Resasco, Redispersion of Pd on acidic supports and loss of methane combustion activity during the selective reduction of NO by CH4, Catal. Lett. 56 (1998) 111–117.
[53] I.N. Filimonov, I.A. Ikonnikov, A.Y. Loginov, EPR investigation of paramagnetic species on palladium-promoted yttria and lanthana, J. Chem. Soc. Faraday Trans. 90 (1994) 219–226.
[54] J. Michalik, M. Narayana, L. Kevan, Studies of the interaction of Pd3+ and Pd+ with organic adsorbates, water, and molecular oxygen in Pd-Ca-X zeolite by electron spin resonance and electron spin-echo modulation spectroscopy, J. Phys. Chem. 89 (1985) 4553–4560.
[55] L.S. Stokes, D.M. Murphy, R.D. Farley, C.C. Rowlands, S. Bailey, EPR investigation of PdI species in palladium-exchanged ZSM-5 and beta zeolites, PCCP 1 (1999) 621–628.
[56] A.K. Ghosh, L. Kevan, Interaction of palladium species with hydrogen, water, and benzene on NaPd-Y and CaPd-Y zeolites studied by electron spin resonance and electron spin echo modulation spectroscopies: further evidence for migration of palladium species, J. Phys. Chem. 94 (1990) 1953–1957.
[57] L. Kevan, Catalytically important metal ion intermediates on zeolites and silica surfaces, Rev. Chem. Intermed. 8 (1987) 53–85.
[58] F. Wyrwalski, J.F. Lamonier, S. Siffert, E.A. Zhilinskaya, L. Gengembre, A. Aboukais, Bulk and surface structures of iron doped zirconium oxide systems—influence of preparation method, J. Mater. Sci. 40 (2005) 933–942.
[59] S. Wright, R.C. Barklie, EPR characterization of defects in monoclinic powders of ZrO2 and HfO2, Mater. Sci. Semicond. Process. 9 (2006) 892–896.
[60] M.I. Ivanovskaya, E.V. Frolova, Nature and conditions of formation of structural defects in zirconium(IV) oxide in the course of its preparation from zirconium hydroxide, Russ. J. Gen. Chem. 77 (2007) 524–531.
[61] E.V. Frolova, M.I. Ivanovskaya, The origin of defects formation in nanosized zirconia, Mate. Sci. Eng.: C 26 (2006) 1106–1110.
[62] F.R. Chen, G. Coudurier, J.F. Joly, J.C. Vedrine, Superacid and catalytic properties of sulfated zirconia, J. Catal. 143 (1993) 616–626.
[63] C.R. Vera, J.C. Yori, J.M. Parera, Tetragonal structure, anionic vacancies and catalytic activity of SO42-ZrO2 catalysts for n-butane isomerization, Appl. Cata. A: Gen. 167 (1998) 75–84.
[64] M. Che, J.F. Dutel, P. Gallezot, M. Prlmet, A study of the chemisorption of nitric oxide on PdY zeolite. Evidence for a room temperature oxidative dissolution of palladium crystallites, J. Phys. Chem. 80 (1976) 1976–2381.
[65] J.-S. Yu, J.-M. Comets, L. Kevan, Electron paramagnetic resonance and electron spin echo modulation spectroscopic studies on the location and adsorbate interactions of paramagnetic Pd ion species in PdII = exchanged K-L zeolite, journal of chemical society, Faraday Trans. 89 (1993) 4397–4403.
[66] J.-S. Yu, L. Kevan, Electron spin resonance analysis of paramagnetic Pd(I) species in Pd(II)-exchanged H-rho zeolite, React. Kinet. Catal. Lett. 57 (1996) 311–321.
[67] S. Praserthdam, P. Wongmaneenil, B. Jongsomjit, Investigation of different modifiers for nanocrystal zirconia on W/ZrO2 catalysts via esterification, J. Ind. Eng. Chem. 16 (2010) 935–940.
[68] L.J. Lobree, A.W. Aylor, J.A. Reimer, A.T. Bell, NO reduction by CH4 in the presence of O2 over Pd-H-ZSM-5, J. Catal. 181 (1999) 189–204.
[69] M. Ogura, M. Hayashi, S. Kage, M. Matsukata, E. Kikuchi, Determination of active palladium species in ZSM-5 zeolite for selective reduction of nitric oxide with methane, Appl. Catal. B: Environ. 23 (1999) 247–257.